Supplemental Figure 1

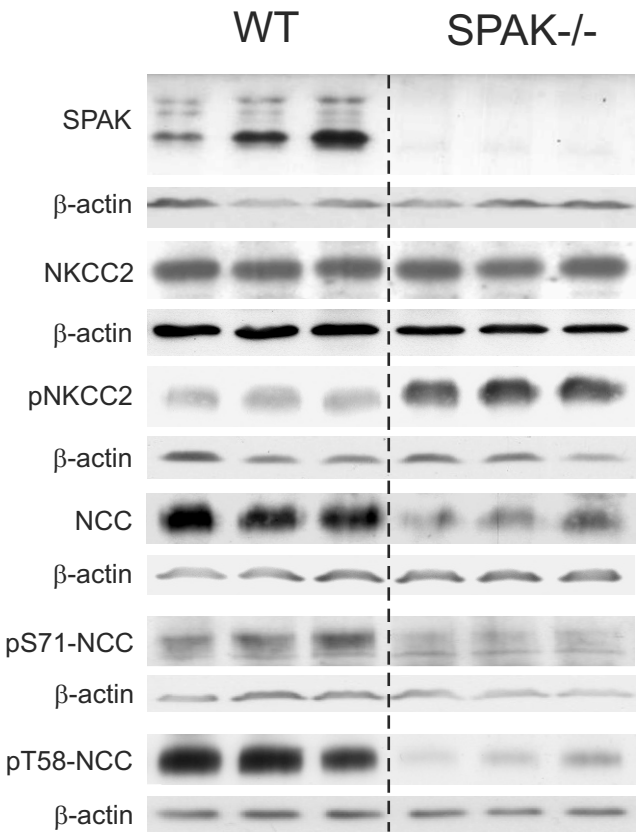

A

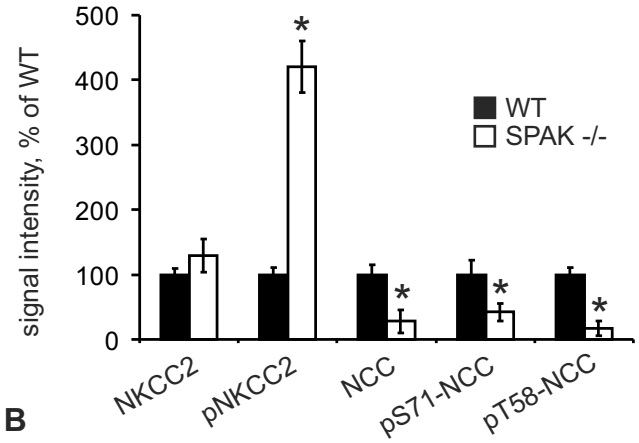

B

Supplemental Figure 2

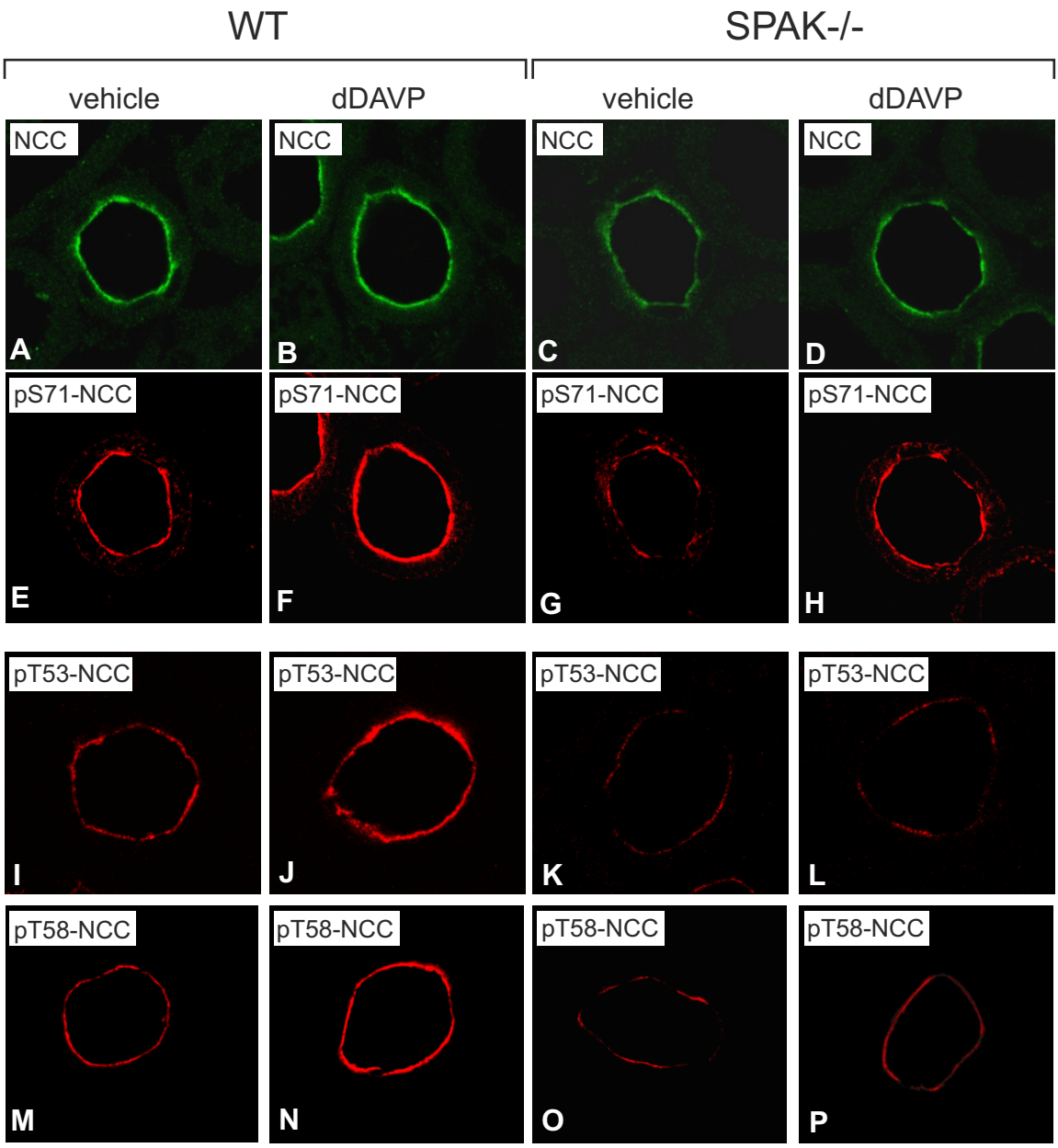

	WT		SPAK-/-	
	vehicle	dDAVP	vehicle	dDAVP
NCC	100±25	111±35	61±7§	62±5
pS71-NCC	100±24	147±6*	65±11§	60±11
pT53-NCC	100±45	263±35*	47±17§	37±13
pT58-NCC	100±32	498±163*	86±36	145±52

Q

Supplemental Figure 3

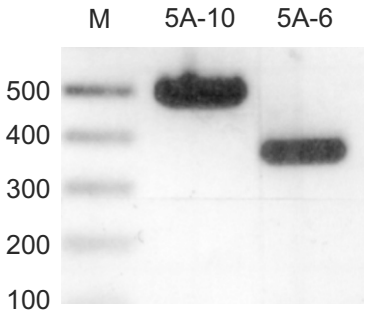

A

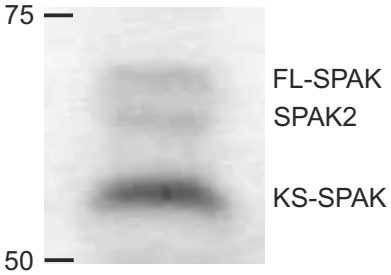

B

AGTCCAGTCACAAGCAGTCTCCTCGGTGAGTGCAG
ACTATCAGCTGGTTGAAACCCCCAGGCTTTGTGGCT
TTGGGTAA**C**TTACCAAAGGACTCATTTCCTTTAGCA
AAGAGTAAAGAAAATATTGCCTTTTACCATTGCTGG
CACACAGTAGGTACACTATATAGCCATCAACGAACG
GTGTTGCTATGGTTACTAGTGTTACCCTCCTCCCTA
ACGTTACTGCAGCCAGCAGGACCACACTTGCGCTG
CCTGGAGGTCATGTGTATGCCAGATTCATCTCGAAA
GAGATTCAGCTCTGAGAGACTGTGAGTTACAAAAAG

C

Supplemental Figure 4

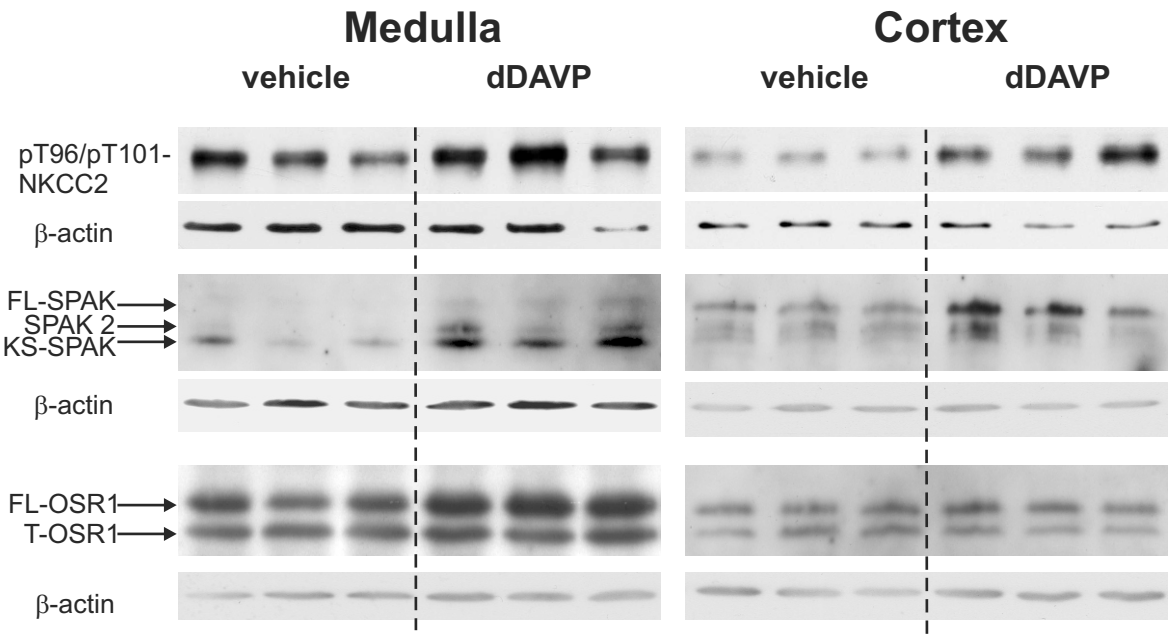

A **B**

product	vehicle, %	dDAVP, %
pT96/pT101-NKCC2	100±31	248±47*
total SPAK	100±38	255±17*
FL-SPAK	100±5	225±11*
SPAK2	100±6	214±63
KS-SPAK	100±15	227±9*
total OSR1	100±4	120±5*
FL-OSR1	100±8	122±7*
T-OSR1	100±6	117±9*

C

product	vehicle, %	dDAVP, %
pT58-NCC	100±19	482±38*
total SPAK	100±25	150±17
FL-SPAK	100±14	195±22*
SPAK2	100±21	106±28
KS-SPAK	100±32	98±35
total OSR1	100±42	89±37
FL-OSR1	100±41	98±36
T-OSR1	100±42	88±29

D

Supplemental Figure 1

Steady state abundance and phosphorylation of NKCC2 and NCC in WT and SPAK-/- mice. (A) Representative immunoblots from WT and SPAK-/- kidney homogenates detected with antibodies to SPAK (three bands between 50 and 75 kDa), NKCC2, pT96/pT101-NKCC2, NCC, pS71-NCC, and pT58-NCC (bands at approximately 160 kDa throughout). Loading was controlled by concomitant detection of β-actin (approximately 40 kDa) as shown below the corresponding immunoblots. (B) Densitometric evaluation of the blots normalized to loading controls. Data are the means ± SD, * $p<0.05$.

Supplemental Figure 2

Acute effects of dDAVP on the abundance and phosphorylation of NCC, confocal evaluation. (A-H) Representative images of DCT profiles from WT and SPAK-/- kidney sections double-stained with anti-NCC and anti-pS71-NCC antibodies after 30 min vehicle or dDAVP treatment. (E-P) Parallel confocal images of DCT profiles labeled with anti-pT53-NCC and anti-pT58-NCC antibodies (concomitant labeling of NCC was performed; not shown). (Q) Evaluation of the confocal signals by intensity. Values obtained in WT after vehicle application set at 100%. Data are the means ± SD; * $p<0.05$ for intrastrain differences (vehicle vs. dDAVP); § $p<0.05$ for interstrain differences (WT vs. SPAK-/- upon vehicle).

Supplemental Figure 3

Verification of KS-SPAK expression and abundance in rat kidney. (A) RT-PCR from total rat kidney RNA using forward primer in the alternative exon 5 (5A) of KS-SPAK and reverse primers in exon 10 (5A-10) or exon 6 (5A-6) produced products of predicted sizes (M = DNA ladder). (B) Immunoblotting from rat kidney homogenates using C-SPAK antibody produced the characteristic three bands corresponding to FL-SPAK, SPAK2, and KS-SPAK. Note high abundance of KS-SPAK. (C) Sequencing of both KS-SPAK PCR products (A) confirmed the expression of this splice variant in rat kidney. Clones contained rat exon 5A fused to rat exon 6. Shaded text indicates location of the forward primer within rat exon 5A; the underlined sequence is homologous to mouse exon 5A.

Supplemental Figure 4

Long term effects of dDAVP on SPAK-OSR1 in Brattleboro rats with diabetes insipidus. (A, B) Representative immunoblots showing SPAK and OSR1 immunoreactive bands in renal medulla containing TAL but not DCT (A) and cortex containing DCT (B) from DI rats after 3 days of vehicle or dDAVP treatment. The effect of dDAVP was confirmed by substantially increased NKCC2- or NCC phosphorylation. β-actin bands below the corresponding immunoblots served as loading controls. (C, D) Densitometric evaluation of single immunoreactive bands from medulla (C) and cortex (D) normalized to loading controls. Note strong signal increases of SPAK isoforms in both renal medulla and cortex compared to modest increases of OSR1 variants in renal medulla only. Data are the means ± SD, * $p<0.05$.